

Tropospheric Zenith Delay Prediction Accuracy for Airborne GPS High-Precision Positioning

V. B. Mendes^{1,2} and R. B. Langley²

¹Faculty of Sciences of the University of Lisbon, R. Ernesto de Vasconcelos, Bloco C1, Piso 3, 1700 Lisboa, Portugal; e-mail: vmendes@lmc.fc.ul.pt. ²Geodetic Research Laboratory, Department of Geodesy and Geomatics Engineering, University of New Brunswick, P.O. Box 4400, Fredericton, N.B., E3B 5A3 Canada; e-mail: lang@unb.ca.

BIOGRAPHY

Virgílio Mendes received his Diploma in Geographic Engineering from the Faculty of Sciences of the University of Lisbon, Portugal, in 1987. Since then, he has been working as a teaching assistant at this university. His principal areas of research are the modeling of tropospheric delay in space techniques and the application of the Global Positioning System to the monitoring of crustal deformation.

Richard Langley is a professor in the Department of Geodesy and Geomatics Engineering at the University of New Brunswick, where he has been teaching and conducting research since 1981. He has a B.Sc. in applied physics from the University of Waterloo and a Ph.D. in experimental space science from York University, Toronto. Dr. Langley is a co-author of the Guide to GPS Positioning and is a contributing editor and columnist for GPS World magazine.

ABSTRACT

When traversing the earth's neutral atmosphere, GPS radio signals are affected significantly by the variability of its refractive index, which causes primarily a delay, usually referred to in the literature as the tropospheric delay. An inaccurate modeling of this delay results in degradation of position estimates, affecting mainly the height component.

The tropospheric delay is commonly divided into two components, "hydrostatic" and "wet", each one consisting of the product of the delay at the zenith and a mapping function that projects the zenith delay onto the desired line-of-sight. A few high-accuracy mapping functions, parameterized by either specific meteorological parameters or other site-dependent parameters, have been developed in recent years. As regards the prediction of the zenith delay, the problem is far more complicated essentially due to the high spatial and temporal variability of the wet component.

We have determined mean bias and r.m.s. scatter for a great number of zenith delay prediction models developed in the last few decades, including the models

generally used in airborne navigation, by comparing the models against ray-tracing using a one-year data set of radiosonde profiles from 50 stations distributed worldwide. We have concluded that the hydrostatic zenith delay can be predicted with submillimetre accuracy, provided accurate measurements of station pressure are available. As regards the wet zenith delay, the models differ significantly in accuracy but show very similar r.m.s. scatter. Our analyses show that the wet zenith delay can typically be predicted with a precision of ~3 cm (at the one-sigma level), using meteorological data. The prediction of the total delay by models typically used in airborne navigation indicates a much poorer accuracy, leading to prediction bias ranging from ~6 cm up to more than 20 cm. In general, all the models tested perform significantly better at mid-latitudes than at low latitudes.

INTRODUCTION

As radio signals used by radiometric space techniques traverse the earth's neutral atmosphere, they experience a decrease in their speed of propagation and, as a consequence of Fermat's principle of least time, a deviation of their path from a straight line. This global effect is generally known as tropospheric propagation delay – as the troposphere is responsible for most of this effect – and is induced by the variable refractive index of the neutral atmosphere.

A mismodeling of the tropospheric delay results in a degradation of the estimates of the height component of position and may therefore constitute a limitation in high-accuracy airborne GPS positioning. Errors due to incorrect tropospheric delay modeling may also introduce errors in carrier phase ambiguity resolution [Mendes et al., 1995]. The modeling of tropospheric delay for precise airborne relative positioning is further complicated due to the large height difference generally existing between the ground-based receiver and the airborne remote receiver. Shi and Cannon [1995] found a significant correlation between the residual effect of tropospheric delay on the estimated height component and the height difference between the reference and remote receivers.

For modeling purposes, the tropospheric delay can be explicitly written as the contribution of a hydrostatic (mostly dry) and a wet component, each one consisting of the product of the delay experienced in the zenith direction and a mapping function that models the elevation angle dependence of the tropospheric delay:

$$d_{\text{trop}} = d_{\text{h}}^z \cdot m_{\text{h}}(\epsilon) + d_{\text{w}}^z \cdot m_{\text{w}}(\epsilon), \quad (1)$$

where d_{trop} is the tropospheric propagation delay at a given elevation angle ϵ , d_{h}^z and d_{w}^z are, respectively, the hydrostatic and wet zenith delays, and $m_{\text{h}}(\epsilon)$ and $m_{\text{w}}(\epsilon)$ are the hydrostatic and wet mapping functions, respectively.

The goal of this paper is to assess models for zenith delay prediction models. For airborne positioning, the mapping functions developed by Niell [1996] are particularly interesting, due to their high-accuracy and independence from meteorological parameters. A large number of mapping functions have been intercompared by Mendes and Langley [1994].

ZENITH DELAY

The delay experienced by a radio signal in the zenith direction is defined as

$$d_{\text{trop}}^z = 10^{-6} \int_{r_s}^{r_a} N \, dz, \quad (2)$$

where N is the refractivity, r_s is the geocentric radius of the receiver antenna, r_a is the geocentric radius of the top of the neutral atmosphere, and dz has length units.

The refractivity of a parcel of air is expressed as [Thayer, 1974]:

$$N = K_1 \left(\frac{P_d}{T} \right) Z_d^{-1} + \left[K_2 \left(\frac{e}{T} \right) + K_3 \left(\frac{e}{T^2} \right) \right] Z_w^{-1}, \quad (3)$$

where K_i are constants empirically determined in laboratory (see Bevis et al. [1994] for a discussion on refractivity constants), P_d is the partial pressure due to dry gases, e is the water vapor pressure, T is the temperature, Z_d and Z_w are the compressibility factors for dry air and water vapor, respectively [Owens, 1967].

The first term on the right-hand side of Equation (3) does not depend on the water vapor content of the atmosphere and is therefore known as the *dry component* of the refractivity; the second term represents the *wet component* of the refractivity.

If we assume that air behaves as an ideal gas, then $P_d = P - e$ and $Z_d = Z_w = 1$; hence Equation (3) is commonly rewritten as

$$N = K_1 \frac{P}{T} + (K_2 - K_1) \frac{e}{T} + K_3 \frac{e}{T^2}. \quad (4)$$

An alternate separation of the refractivity components was derived by Davis et al. [1985]. They rewrite Equation (3) as:

$$N = K_1 R_d \rho + K_2' \left(\frac{e}{T} \right) Z_w^{-1} + K_3 \left(\frac{e}{T^2} \right) Z_w^{-1}, \quad (5)$$

where

$$K_2' = K_2 - K_1 \left(\frac{R_d}{R_w} \right), \quad (6)$$

R_d is the specific gas constant for dry air, R_w is the specific gas constant for water vapor, and ρ is the density of moist air.

The first term of the right-hand side of Equation (5) is no longer purely “dry”, as there is a contribution of the water vapor hidden in the total density, and is known in the literature as the “hydrostatic” component of refraction. On the other hand, the “wet” component is also different from the wet component of the “dry/wet” formalism, as a consequence of the different partitioning of dry gases and water vapor contributions; it should probably be referred to as the “non-hydrostatic” component, but the term “wet” is still commonly used. In this paper, the designation “wet” will also be used and therefore no distinction between the wet and non-hydrostatic components will be made, but it is important to note that these are actually two (slightly) different quantities.

If we consider the refractivity to be composed of a hydrostatic and a wet component, the zenith delay can therefore be split into two components, denominated the *hydrostatic zenith delay* and the *wet zenith delay* and consequently Equation (2) can be written as:

$$d_{\text{trop}}^z = 10^{-6} \int_{r_s}^{r_a} N_h \, dz + 10^{-6} \int_{r_s}^{r_a} N_w \, dz, \quad (7)$$

or symbolically,

$$d_{\text{trop}}^z = d_{\text{h}}^z + d_{\text{w}}^z, \quad (8)$$

where d_{h}^z represents the hydrostatic zenith delay and d_{w}^z represents the wet zenith delay. With regards to the hydrostatic component, we have specifically:

$$d_{\text{h}}^z = 10^{-6} K_1 R_d \int_{r_s}^{r_a} \rho \, dz. \quad (9)$$

Using the hydrostatic equation, we can derive the following relation:

$$d_{\text{h}}^z = 10^{-6} K_1 R_d \frac{P_s}{g_m}, \quad (10)$$

where g_m is the acceleration due to gravity at the center of mass of the vertical column of air, and P_s is the pressure at the antenna location.

For the wet component, we write:

$$d_w^z = 10^{-6} \int_{r_s}^{r_a} \left[K_2' \left(\frac{e}{T} \right) + K_3 \left(\frac{e}{T^2} \right) \right] Z_w^{-1} dz. \quad (11)$$

The direct solution of this integral requires a water vapor profile, which is generally not known, and surface conditions are not universally strongly correlated with the conditions aloft. Nevertheless, a large variety of models attempting to tackle this problem have been developed and a new empirical model will be presented here.

A NEW MODEL

Before reviewing the existing zenith delay models we have assessed in our study (see Appendix I), we present a new empirical model for the wet zenith delay.

Based on ray-tracing results obtained using data from 50 radiosonde stations distributed worldwide (see Appendix II for locations) for all of 1992, we have found that there is a correlation between the wet zenith delay and surface water vapor pressure (a correlation that varies from weak to strong, depending on the location), which can be expressed by the following model (labeled UNB98ZW, for discussion purposes):

$$d_w^z = 0.0122 + 0.00943e \quad (12)$$

where d_w^z is given in metres and e in hectopascals. The coefficients for this model were obtained from a least-squares fit with 10,822 data points (sampled from the total number of traces). The uncertainties for the intercept and slope of the straight line are 4.1×10^{-4} m and 2.9×10^{-5} m hPa⁻¹, respectively. The r.m.s. of the fit was 0.024 m.

For airborne GPS navigation, and for many other applications, accurate meteorological data may be difficult to acquire and therefore the use of wet zenith delay prediction models using meteorological data as an input may be inconvenient or even impossible. In the case of our model, the use of the water vapor pressure as the only input would nevertheless require measurements, e.g., of temperature and relative humidity (as water vapor pressure is typically not measured directly), at each given height. There are however several sources of mean values of water vapor pressure, such as the International Organization for Standardization Reference Atmospheres for Aerospace Use (hereafter ISO) [ISO, 1982; 1983], that can be used to by-pass that difficulty. Values are available for the months of January and July, and for altitudes ranging from 0 m to 10,000 m (every 1,000 m) and for the following latitudes in the northern hemisphere: 10°, 30°, 50°, and 70°.

Using this information, we have developed a model that allows the determination of water vapor pressure at a given latitude, height, and day-of-year. We fitted a model to the tabulated values of water vapor pressure of the ISO atmospheres, and subsequently, we carry out an interpolation to a given day-of-year using a scheme that follows the one adopted by Niell [1996] in the development of his mapping functions (for details see Mendes [1998]).

OTHER MODELS

Our model has been incorporated into an analysis of 12 different wet zenith delay models. We have also assessed hydrostatic and total zenith delay models, all of which are briefly described in this section.

If we follow a theoretical approach, the modeling of the hydrostatic zenith delay is straightforward, and models can only differ due to the choice of the refractivity constant (the effect of choosing different refractivity constants is not significant however) and on the modeling of the height and latitude dependence of the acceleration of gravity. Saastamoinen [1973] and Baby et al. [1988] have developed models based on this approach (see Equation (10)). Hopfield [1969] showed that the dry zenith delay could also be obtained using a quartic model for the dry refractivity profile and developed the following model:

$$d_d^z = 10^{-6} N_{ds} \frac{H_d^e - H_s}{5}, \quad (13)$$

where N_{ds} is the surface dry refractivity, H_s is the station height, and H_d^e is the so-called equivalent height, which can be determined as a function of surface temperature [Hopfield, 1972].

For the wet zenith delay we have chosen a much larger selection of models. This choice embraces models based either on theoretical assumptions concerning water vapor height profiles or on empirical models. In general, these models are highly dependent on the water vapor pressure at the antenna location. Appendix I lists the models selected for this intercomparison study and shows the input parameters used by each one. The models have been used in their standard formulation and driven by the surface meteorological data provided by the radiosonde soundings. In order to provide reliable information on temperature lapse rate needed for some models, monthly-averaged values were computed for all stations.

The Hopfield model is formulated on the assumption that the wet refractivity can also be described by the quartic profile (for convenience, as physically this is not justified). The wet equivalent height was set to a fixed value [Hopfield, 1972].

Saastamoinen [1973] and Askne and Nordius [1987] assumed that the water vapor pressure decreases with height according to a power law. In its full expression,

the Saastamoinen model can be tailored to a particular location (see Janes et al. [1991]); the model analyzed here corresponds to the standard formulation derived for mid-latitude conditions. For the model developed by Askne and Nordius, the global value of the water vapor lapse parameter (λ) given by Smith [1966] was used (this parameter can be tuned for a particular region). Collins et al. [1996] used this model as the basis of the UNB3w wet zenith delay model, where values for the input meteorological parameters are obtained by interpolation through a set of average values for different latitudes (a lookup table), compiled from different sources. In its full implementation, the hydrostatic component of UNB3 is modeled by the Saastamoinen model, using a lookup table of average values of surface pressure, and the elevation dependence of the delay is modeled with the mapping functions developed by Niell [1996].

Callahan [1973] assumes an exponential height profile for the water vapor pressure (empirically determined). In its simplest form, the model is only a function of the surface water vapor pressure and temperature. Chao [1973] based his model on an adiabatic atmosphere model, and derived an expression that is a function of surface water vapor pressure and temperature, and temperature lapse rate.

Berman [1976] and Baby et al. [1988] have derived models (codes B70w and BB1w, in Appendix I) that basically share the same assumptions: the relative humidity is constant with altitude (and equal to its surface value) up to a certain height and the temperature decreases with height at a constant rate. The models differ in the computation of the water vapor pressure (Baby et al. proposed two models for this computation, and the simplest one was used in BB1w). They also proposed empirical models – B74w (Berman 74), BTMw (Berman TMOD), and BB2w. The Berman empirical models are based on the existence of a strong linear relation between the ratios of the wet and hydrostatic delays and corresponding refractivities. The empirical model by Baby et al. is a function of surface relative humidity and temperature, and a set of empirical coefficients (ν and γ), which can be adjusted for different climatic regions (the global values were used in our analysis).

Ifadis [1986] found a weak correlation between the wet zenith delay and all “standard” surface meteorological parameters (temperature, pressure, and water vapor pressure) and, as with UNB98ZW (98aw), is based on ray tracing through radiosonde data (but in our model only the water vapor pressure dependence is considered).

Finally, we have also included in our analysis a version of UNB98ZW driven by our model for determination of water vapor pressure (98bw). This version and UNB3 are therefore the only models analyzed whose use is totally independent of concurrently-measured meteorological data.

The total delay at the zenith is formally obtained by adding the contributions of the hydrostatic and wet zenith delay models. However, some models do not have an explicit separation of the hydrostatic and the wet components. Such is the case of most of the models specifically developed for airborne positioning. In general, these models are also independent of direct measurements of meteorological data. The models incorporated in GPS receivers have generally a simple mathematical structure that allow fast computations by the task-limited microprocessor. Other models are more sophisticated and constitute, in general, analytical approximations to refractivity profile models.

Another feature of these models is that they also incorporate a mapping function. The zenith delay component is therefore obtained by taking the value of such “hybrid models” in the direction of the zenith.

We have selected one model known to be used in GPS receivers, three models used in “precise” airborne navigation, and the Saastamoinen model (a combination of the hydrostatic and wet zenith delay models, to be used as reference).

The model we have selected as representative of models used in GPS receivers is documented in the literature (e.g. Braasch [1990]; Lewandowski et al. [1992]), but the original source of the model is unknown to us. Lewandowski et al. [1992] state that it is “*implemented in receivers manufactured by Stanford Telecommunication Inc.*”. We will label it as STI. The only input for this model is the user’s height.

Another commonly-used model is the one developed by Altshuler and Kalaghan [1974]. This model is a function of the user’s latitude, height, and surface refractivity, which is in turn estimated as a function of the user’s latitude, height, and season.

The zenith delay model adopted for the NATO standard troposphere model [NATO, 1993] is based on the CRPL Reference Atmosphere - 1958 [Bean and Thayer, 1959] and is a function of the height above sea level and the mean sea-level refractivity (a fixed value of 324.8 N-units was used).

The Federal Aviation Administration (FAA) initially proposed a model for the Wide Area Augmentation System (WAAS) that is derived from the Altshuler and Kalaghan model [DeCleene, 1995]. The input for this model is the user’s height above sea level, station latitude, and day-of-year.

MODEL ASSESSMENT

As benchmark values for model assessment we have used ray tracing through the radiosonde data used for the UNB98ZW model development, but the total number of traces (32,467) was considered. The radiosonde stations have heights above sea level ranging from 3 m to 2234 m and have typically two radiosonde launches per day (at 0^h and 12^h UTC).

Radiosonde soundings consist of height profiles of pressure, temperature, and relative humidity or dew-point.

The performance of each prediction model was assessed in terms of its bias, corresponding to the mean of the differences between the model values and ray tracing, and root-mean-square (r.m.s.) scatter about this mean value (standard deviation). To assess the global performance (total number of traces) we have adopted a representation by box-and-whisker plots, where the following statistical quantities are represented: median and mean (thinner and thicker lines inside the boxes, respectively), 25th and 75th percentiles (vertical box limits), 10th and 90th percentiles (whiskers), and 5th and 95th percentiles (open circles). We have assessed the performance of the hydrostatic delay, wet delay, and total delay models separately.

HYDROSTATIC ZENITH DELAY

The results of our global assessment are presented in Figure 1 (for codes used in the figures see Appendix I).

The outstanding performance of the Saastamoinen model is very clear, with submillimetre bias and submillimetre r.m.s. scatter with respect to our benchmark values. The other two models show biases of 3-4 mm and r.m.s. scatter of 2-3 mm.

The performance of each model at the different radiosonde stations is shown in Figure 2.

The bias of each model is clearly dependent on the latitude of the station, even though it may be

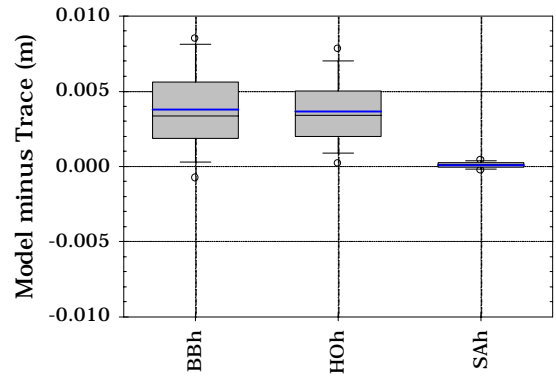


Figure 1 – Box-and-whisker plot for the differences between the hydrostatic zenith delay models and ray tracing.

considered insignificant for the Saastamoinen model. The latitude-dependent bias seen for the Hopfield model is probably explained by an inadequate value of the equivalent dry height (an error of 100 m in this value induces a bias of about 5 mm in delay), but other effects may also be responsible for these biases. The r.m.s. scatter (1-2 mm) is within the values quoted by Hopfield [1972] and again is likely connected to variations in dry equivalent height, judging by the small r.m.s. scatter attained at stations with a very steady surface temperature.

The Baby et al. model performs similarly to the Hopfield model in terms of mean bias, but has an r.m.s. scatter which is comparable to that obtained for the Saastamoinen model. The source of the bias in this

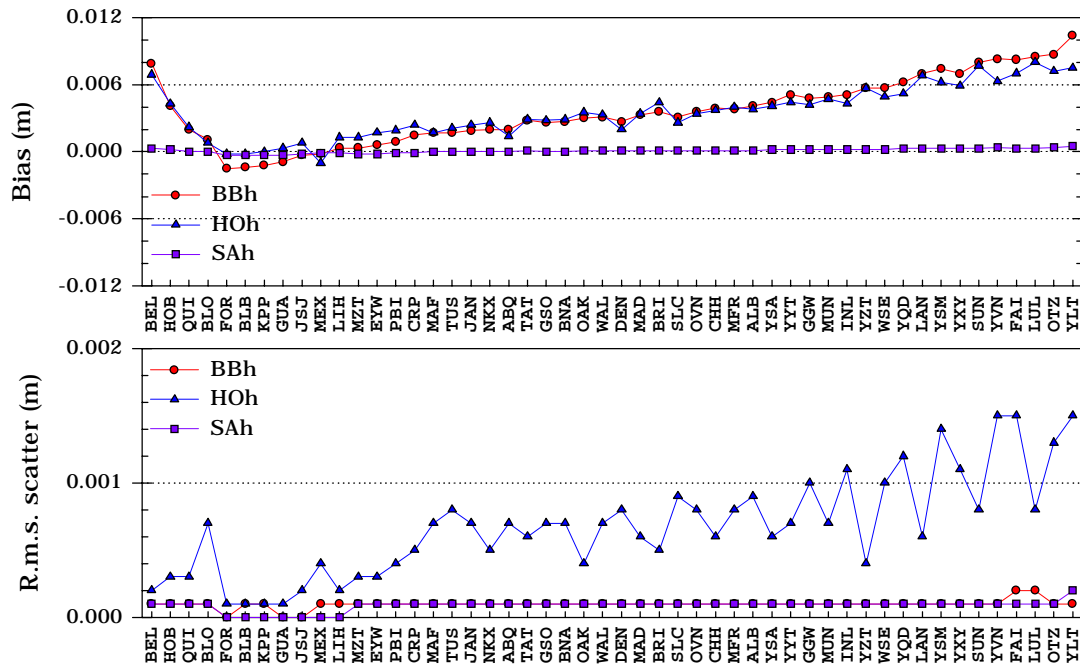


Figure 2 – Bias (top plot) and r.m.s. scatter (bottom plot) for the hydrostatic zenith delay models, for 50 radiosonde stations.

model is associated with their gravity modeling approach. The model used by Baby et al. to estimate g_m is a function of different quantities, such as surface temperature and temperature lapse rate. The values for the temperature lapse rate used in our analysis are monthly-averaged values determined at each station, which minimizes the influence of errors due to lapse rate determination.

The Hopfield and the Baby et al. models tend to over-predict the zenith delay, except for the equatorial region. The Saastamoinen performance is extremely good for all the analyzed radiosonde stations and it is therefore expected that this model will provide very accurate predictions of the hydrostatic zenith delay given accurate station pressures.

WET ZENITH DELAY

For the group of models driven by meteorological data, and despite the heterogeneity of models, the global analysis allows us to infer that the models show different biases but very similar r.m.s. scatter, except for Berman 74, Berman TMOD and Callahan, which achieve the worst performance of this major group (see Figure 3).

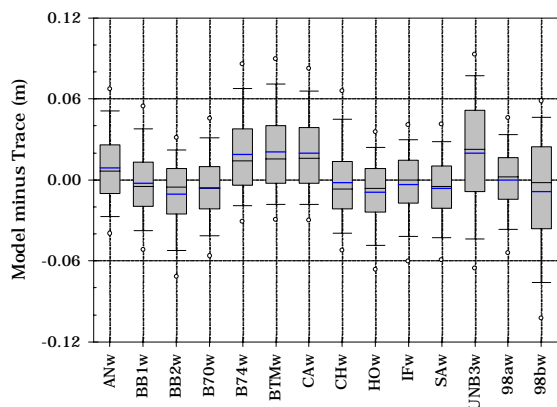


Figure 3 – Box-and-whisker plot for the differences between the wet zenith delay models and ray tracing.

The best overall performance is achieved by our model (UNB98ZW). This is partially due to the fact that we have used part of the radiosonde data to derive the coefficients for the model, resulting therefore in an essentially zero mean bias. The r.m.s. scatter (slightly less than 3 cm) is also the lowest, by a very small margin.

The two models requiring no external meteorological data (98bw and UNB3w) also perform similarly in terms of r.m.s. scatter, but 98bw has a much lower mean bias. As compared to the best models using meteorological data, 98bw and UNB3w see the r.m.s. scatter increased by a factor of ~1.6.

None of the models has a clear advantage at all radiosonde stations used in our intercomparison, as illustrated in Figure 4. The histograms in this figure represent the percentage of best performances accomplished by the different models on a station-by-station basis, in terms of bias, r.m.s. scatter, and total error (resulting from the combination of the bias and r.m.s. scatter). In terms of bias, we can conclude that there is a good distribution of best rankings, with some advantage for the group ANw, BB2w, SAw, and 98aw. BB1w achieves the best performance as regards the r.m.s. scatter, but the differences in r.m.s. scatter between this model and most of the best models is at the sub-millimetre level. When we examine the total error, the advantage of UNB98ZW is to be noted. The models developed by Askne and Nordius and Baby et al. have identical performance according to this criterion.

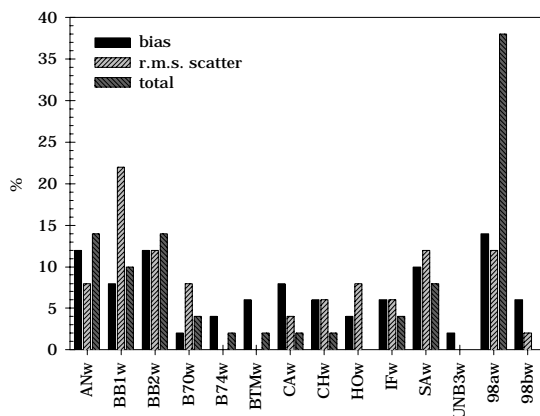


Figure 4 – Histogram for the best performances, in percentage.

Of special interest for airborne applications is the performance of the two models using no external meteorological data. These perform very differently according to the latitude of the station. In general, the UNB3w model performs better for low-latitude stations, whereas 98bw performs better for middle and high latitudes, as illustrated in Figure 5. The 98bw model performs better than UNB3w for about 2/3 of the total number of stations, for any of the ranking criteria. The poorer performance of the 98bw model at low-latitudes can be explained by inadequate values of water vapor pressure given in the ISO standard atmospheres. For the common latitude of 30° N, the water vapor pressure of the ISO Reference Atmosphere is more than 20% lower than the value we have computed from the U.S. Standard Atmosphere Supplements, 1966 (USSA) [ESSA/NASA/USAF, 1966]. It is therefore possible that a combination of the information provided by both standard atmospheres could lead to an improvement of our model for water vapor pressure determination.

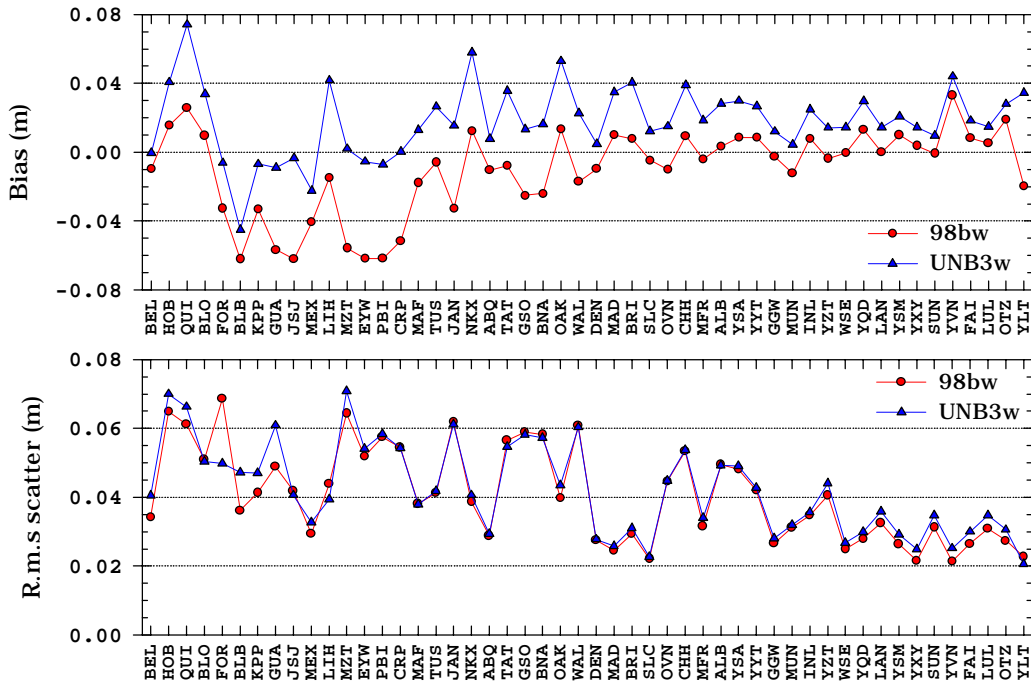


Figure 5 – Bias (top plot) and r.m.s. scatter (bottom plot) for UNB3w and UNB98WZ wet zenith delay models, for 50 radiosonde stations.

TOTAL ZENITH DELAY

For the total zenith delay models, the box-and-whisker plot for the total number of differences with respect to ray tracing shown in Figure 6 indicates that the models commonly used in navigation applications perform poorly both in an absolute sense (with respect to our benchmark values) and in a relative sense, when compared with the Saastamoinen model.

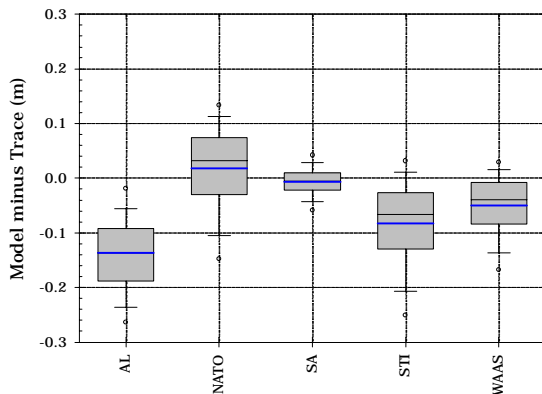


Figure 6 – Box-and-whisker plot for the differences between the total zenith delay models and ray tracing.

Among the models used in navigation applications, the NATO and initially-proposed WAAS models perform the best, the latter showing a larger bias but a lower r.m.s. scatter. The large r.m.s. scatter of the NATO model is likely associated with the use of a fixed mean value for surface refractivity. In the case of the

Altshuler and Kalahan model, the use of the refractivity as computed from meteorological data improved the mean bias, but did not improve the r.m.s. scatter, in general.

All the navigation models experience large biases at low-latitude stations, as shown in Figure 7 (the Altshuler and Kalahan model is not shown in these plots, for the sake of clarity of the figure). In the case of the STI model, these biases reach more than 20 cm, but the model performs acceptably at high latitudes, with small mean offsets. The r.m.s. scatter for this model is the same as that obtained for the NATO model, as the only variable in these models is the height of the station. We conclude that the NATO model performs reasonably well at mid-latitudes but degrades towards high and low latitudes. The r.m.s. scatter for this model is larger than that obtained for the WAAS model, which also has a better performance at high latitudes.

CONCLUSIONS

Using ray tracing through a large number of radiosonde profiles, for the year 1992, we have evaluated the performance of different models for tropospheric zenith delay prediction. We have concluded that the hydrostatic zenith delay can be determined from measurements of station pressure with sub-millimetre accuracy, using the Saastamoinen model. The models used for wet zenith delay prediction have serious limitations, due to the high temporal and spatial variability of the wet delay. All models have r.m.s. scatter at the few centimetre-level, even if driven by

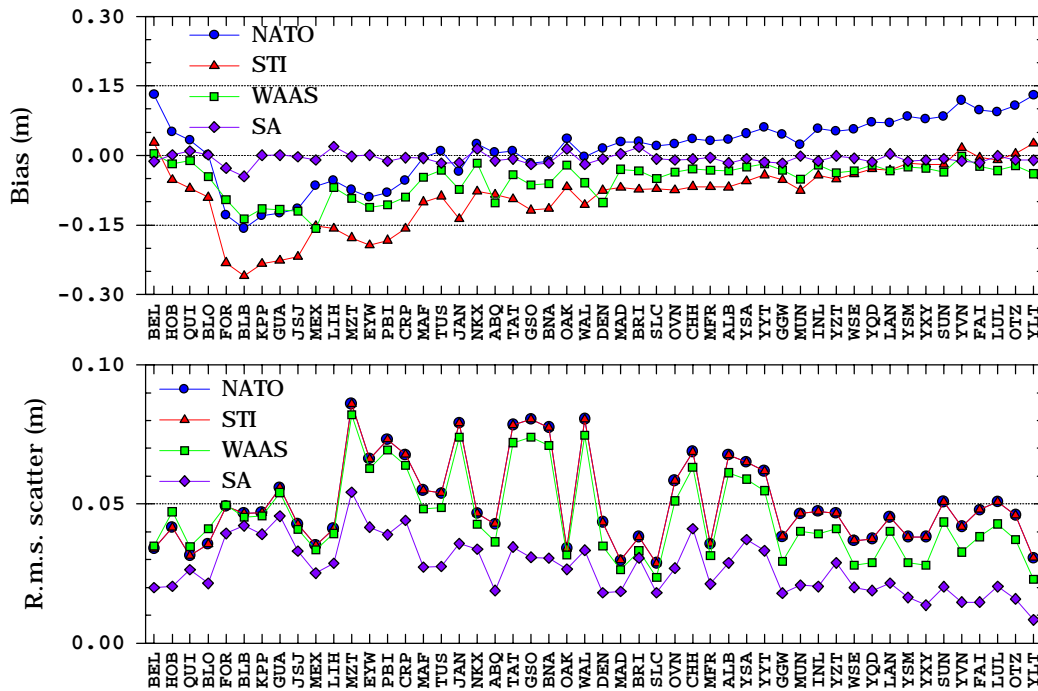


Figure 7 – Bias (top plot) and r.m.s. scatter (bottom plot) for total zenith delay models, for 50 radiosonde stations.

station meteorological data. We have developed a simple model that shows an overall best performance, for different climatic conditions. The model degrades somewhat if driven by average values from standard atmospheres (rather than actual station water vapor measurements), both in bias and r.m.s. scatter. For this variant of our model, the r.m.s. scatter increases by a factor of ~1.6 (up to ~5 cm), but the bias is only unsatisfactory for low latitudes. It has however the advantage of being totally independent of direct meteorological measurements, which is likely the situation encountered in most airborne positioning. The models frequently used in navigation applications presented severe limitations. Even though a clear improvement in r.m.s. scatter cannot be expected for models not using meteorological data, a better calibration for reduction of the bias has to be considered in order to meet the requirements of high-precision airborne positioning.

ACKNOWLEDGMENTS

We would like to express our appreciation to Arthur Niell, for providing us with some of the radiosonde data we used and the ray-trace software (developed by James Davis, Thomas Herring, and Arthur Niell), and to Gunnar Elgered and the Swedish Meteorological and Hydrological Institute, for providing us radiosonde data for some Scandinavian stations.

The support of the “Laboratório de Tectonofísica e Tectónica Experimental” is gratefully acknowledged.

REFERENCES

- Altshuler, E.E. and P.M. Kalaghan (1974). “Tropospheric range error corrections for the NAVSTAR system.” AFCRL-TR-74-0198, Air Force Cambridge Research Laboratories, Bedford, Mass.
- Askne, J. and H. Nordius (1987). “Estimation of tropospheric delay for microwaves from surface weather data.” *Radio Science*, Vol. 22, No. 3, pp. 379-386.
- Baby, H.B., P. Golé, and J. Lavernat (1988). “A model for the tropospheric excess path length of radio waves from surface meteorological measurements.” *Radio Science*, Vol. 23, No. 6, pp. 1023-1038.
- Bean, B.R. and G.D. Thayer (1959). “Models of the atmospheric radio refractive index.” *Proceedings of Institute of Radio Engineers*, Vol. 47, pp. 740-755.
- Berman, A.L. (1976). “The prediction of zenith range refraction from surface measurements of meteorological parameters.” JPL Technical Report 32-1602, Jet Propulsion Laboratory, Pasadena, Calif.
- Bevis, M., S. Businger, S. Chiswell, T.A. Herring, R.A. Anthes, C. Rocken, and R.H. Ware (1994). “GPS meteorology: Mapping zenith wet delays onto precipitable water.” *Journal of Applied Meteorology*, Vol. 33, No. 3, pp. 379-386.
- Braasch, M.S. (1990). “A signal model for GPS.” *Navigation*, Journal of The Institute of Navigation (U.S.), Vol. 37, No. 4, pp. 363-377.

- Callahan, P.S. (1973). "Prediction of tropospheric wet-component range error from surface measurements." JPL Technical Report 32-1526, Vol. XVIII, pp. 41-46, Jet Propulsion Laboratory, Pasadena, Calif.
- Chao, C.C. (1973). "A new method to predict wet zenith range correction from surface measurements." JPL Technical Report 32-1526, Vol. XIV, pp. 33-41, Jet Propulsion Laboratory, Pasadena, Calif.
- Collins, J.P., R.B. Langley, and L. LaMance (1996). "Limiting factors in tropospheric propagation delay error modelling for GPS airborne navigation." *Proceedings of The Institute of Navigation 52nd Annual Meeting*, Cambridge, Mass., 19-21 June, pp. 519-528.
- Davis, J.L., T.A. Herring, I.I. Shapiro, A.E.E. Rogers, and G. Elgered (1985). "Geodesy by radio interferometry: Effects of atmospheric modeling errors on estimates of baseline length." *Radio Science*, Vol. 20, No. 6, pp. 1593-1607.
- DeCleene, B. (1995). Personal communication, Federal Aviation Administration, May.
- ESSA/NASA/USAF (Environmental Science Services Administration, National Aeronautics and Space Administration, and United States Air Force) (1966). *U.S. Standard Atmosphere Supplements, 1966*. U.S. Government Printing Office, Washington, D.C.
- Hopfield, H.S. (1969). "Two-quartic tropospheric refractivity profile for correcting satellite data." *Journal of Geophysical Research*, Vol. 74, No. 18, pp. 4487-4499.
- Hopfield, H.S. (1972). "Tropospheric refraction effects on satellite range measurements." *APL Technical Digest*, Vol. 11, No. 4, pp. 11-19.
- Ifadis, I. (1986). "The atmospheric delay of radio waves: Modeling the elevation dependence on a global scale." Technical Report No. 38L, School of Electrical and Computer Engineering, Chalmers University of Technology, Göteborg, Sweden.
- International Organization for Standardization (ISO) (1982). *Reference Atmospheres for Aerospace Use*. ISO International Standard 5878-1982, Technical Committee ISO/TC 20, International Organization for Standardization, Geneva, Switzerland.
- International Organization for Standardization (ISO) (1983). *Reference Atmospheres for Aerospace Use, Addendum 2: Air Humidity in the Northern Hemisphere*. ISO International Standard 5878-1982/Addendum 2-1983, Technical Committee ISO/TC 20, International Organization for Standardization, Geneva, Switzerland.
- Janes, H.W., R.B. Langley, and S.P. Newby (1991). "Analysis of tropospheric delay prediction models: Comparisons with ray tracing and implications for GPS relative positioning." *Bulletin Géodésique*, Vol. 65, No. 3, pp. 151-161.
- Lewandowski, W., G. Petit, and C. Thomas (1992). "GPS standardization for the needs of time transfer." *Proceedings of the 6th European Frequency and Time Forum*, Noordwijk, The Netherlands, 17-19 March, ESA SP-340, pp. 243-248.
- Mendes, V.B. (1998). "Modeling the neutral-atmosphere propagation delay in radiometric space techniques." Ph.D. dissertation (in preparation), Department of Geodesy and Geomatics Engineering, University of New Brunswick, Fredericton, New Brunswick.
- Mendes, V.B. and R.B. Langley (1994). "A comprehensive analysis of mapping functions used in modeling tropospheric propagation delay in space geodetic data." *Proceedings of KIS94, International Symposium on Kinematic Systems in Geodesy, Geomatics and Navigation*, Banff, Canada, August 30 - September 2, The University of Calgary, Calgary, Canada, pp. 87-98.
- Mendes, V.B., P. Collins, and R.B. Langley (1995). "The effect of tropospheric propagation delay errors in airborne GPS precision positioning." *Proceedings of ION GPS-95, the 8th International Technical Meeting of the Satellite Division of The Institute of Navigation*, Palm Springs, Calif., 12-15 September, pp. 1681-1689.
- NATO (North Atlantic Treaty Organization) (1993). Standardization Agreement (STANAG) Doc. 4294 EL (Edition 1), Appendix 6 to Annex A, pp. A-6-34 - A-6-37. North Atlantic Treaty Organization, Brussels.
- Niell, A.E. (1996). "Global mapping functions for the atmosphere delay at radio wavelengths." *Journal of Geophysical Research*, Vol. 101, No. B2, pp. 3227-3246.
- Owens, J.C. (1967). "Optical refractive index of air: Dependence on pressure, temperature and composition." *Applied Optics*, Vol. 6, No. 1, pp. 51-59.
- Saastamoinen, J. (1973). "Contributions to the theory of atmospheric refraction." In three parts. *Bulletin Géodésique*, No. 105, pp. 279-298; No. 106, pp. 383-397; No. 107, pp. 13-34.
- Shi, J. and M.E. Cannon (1995). "Critical error effects and analysis in carrier phase-based airborne GPS positioning over large areas." *Bulletin Géodésique*, Vol. 69, No. 4, pp. 261-273.
- Smith, W.L. (1966). "Note on the relationship between total precipitable water and surface dew point." *Journal of Applied Meteorology*, Vol. 5, pp. 726-727.
- Thayer, G.D. (1974). "An improved equation for the radio refractive index of air." *Radio Science*, Vol. 9, No. 10, pp. 803-807.

Appendix I – Codes, references, and input parameters for the analyzed zenith delay models (e – water vapor pressure; T – temperature; P – total pressure; α – temperature lapse rate; doy – day-of-year; ϕ – station latitude; H – height above sea level; g – surface gravity; U – relative humidity; λ , v , and γ – empirical coefficients).

Code	Reference	e	T	P	α	doy	ϕ	H	other
BBh	Baby et al. [1988]		✓	✓	✓		✓	✓	g
HOh	Hopfield [1972]		✓	✓					
SAh	Saastamoinen [1973]			✓			✓	✓	
ANw	Askne and Nordius [1987]	✓	✓		✓		✓	✓	λ
BB1w	Baby et al. [1988]		✓		✓		✓		U
BB2w	Baby et al. [1988]		✓				✓		U, v, γ
B70w	Berman [1976]	✓	✓		✓				
B74w	Berman [1976]	✓	✓						
BTMw	Berman [1976]	✓	✓						
CAw	Callahan [1973]	✓	✓						
CHw	Chao [1973]	✓	✓		✓				
HOw	Hopfield [1972]	✓	✓						
IFw	Ifadis [1986]	✓	✓	✓					
SAw	Saastamoinen [1973]	✓	✓						
UNB3w	Collins et al. [1996]					✓	✓	✓	
98aw	This paper	✓							
98bw	This paper					✓	✓	✓	
AL	Altshuler and Kalaghan [1974]					✓	✓	✓	
NATO	NATO [1993]							✓	
SA	Saastamoinen [1973]	✓	✓	✓			✓	✓	
STI	Lewandowski et al. [1992]							✓	
WAAS	DeCleene [1995]					✓	✓	✓	

Appendix II – Approximate location of radiosonde stations.

STATION	CODE	ϕ ($^{\circ}$ N)	λ ($^{\circ}$ E)	H(m)
Bellingshausen, BAT	BEL	-62.20	-58.93	46
Hobart, Tasmania, Australia	HOB	-42.83	147.50	28
Quintero, Chile	QUI	-32.78	-71.52	8
Bloemfontein, South Africa	BLO	-29.10	26.30	1359
Fortaleza, Brazil	FOR	-3.72	-38.55	19
Balboa, Panama	BLB	8.98	-79.60	66
Trinidad, Trinidad and Tobago	KPP	10.58	-61.35	12
Guam, Mariana Islands, USA	GUA	13.55	144.83	111
San Juan, Puerto Rico	JSJ	18.43	-66.00	3
Mexico City, Mexico	MEX	19.43	-99.07	2234
Lihue, HI, USA	LIH	21.98	-159.35	36
Mazatlan Sinaloa, Mexico	MZT	23.18	-106.42	4
Key West, FL, USA	EYW	24.55	-81.75	3
West Palm Beach, FL, USA	PBI	26.68	-80.12	7
Corpus Christi, TX, USA	CRP	29.77	-97.50	14
Midland, TX, USA	MAF	31.93	-102.20	873
Tuscon, AZ, USA	TUS	32.12	-110.93	788
Jackson, MS, USA	JAN	32.32	-90.07	91
Miramar, CA, USA	NKX	32.87	-117.15	147
Albuquerque, NM, USA	ABQ	35.05	-106.62	1619
Tateno, Japan	TAT	36.05	140.13	27
Greensboro, NC	GSO	36.08	-79.95	277
Nashville, TN, USA	BNA	36.25	-86.57	180
Oakland, CA, USA	OAK	37.75	-122.22	6
Wallops Island, VA, USA	WAL	37.93	-75.48	13
Denver, CO, USA	DEN	39.77	-104.88	1611
Madrid, Spain	MAD	40.50	-3.58	633
Brindisi, Italy	BRI	40.65	17.95	15
Salt Lake City, UT, USA	SLC	40.77	-111.97	1288
Omaha, NE, USA	OVN	41.37	-96.02	400
Chatham, MA, USA	CHH	41.67	-69.97	16
Medford, OR, USA	MFR	42.37	-122.87	397
Albany, NY, USA	ALB	42.75	-73.80	85
Sable Island, NS, Canada	YSA	43.93	-60.02	4
St. John's, NF, Canada	YYT	47.67	-52.75	140
Glasgow, MT, USA	GGW	48.22	-106.62	696
Munich, Germany	MUN	48.25	11.58	484
International Falls, MN, USA	INL	48.57	-93.38	359
Port Hardy, BC, Canada	YZT	50.68	-127.37	17
Edmonton, AB, Canada	WSE	53.55	-114.10	766
The Pas, MB, Canada	YQD	53.97	-101.10	273
Landvetter, Sweden	LAN	57.67	12.30	155
Ft. Smith, NWT, Canada	YSM	60.03	-111.95	203
Whitehorse, YK, Canada	YXY	60.72	-135.07	704
Sundsvall, Sweden	SUN	62.53	17.45	6
Iqaluit, NWT, Canada	YVN	63.75	-68.55	21
Fairbanks, AK, USA	FAI	64.82	-147.87	135
Lulea, Sweden	LUL	65.55	22.13	34
Kotzebue, AK, USA	OTZ	66.87	-162.63	5
Alert, NWT, Canada	YLT	82.50	-62.33	66